

Electronic Supplementary Information (ESI) for

Binder-free CNT network/MoS₂ composite as high performance anode material in lithium ion battery

Congxiang Lu,^{ab†} Wen-wen Liu^{b†}, Hong Li^c and Beng Kang Tay ^{*ab}

^a CINTRA CNRS/NTU/THALES, Nanyang Technological University, Singapore 637553.

^b Novitas, Nanoelectronics Centre of Excellence, School of Electrical and Electronic Engineering, Nanyang Technological University, Singapore 639798.

^c Department of Mechanical Engineering, Stanford University, California 94305, United States.

†These two authors contribute equally to this work.

1. Experimental

As indicated in Fig. 1, the fabrication process of carbon nanotube (CNT)/MoS₂ composite mainly involves three steps: substrate preparation, growth of CNT network fulfilled by CVD and MoS₂ synthesized by hydrothermal reaction.

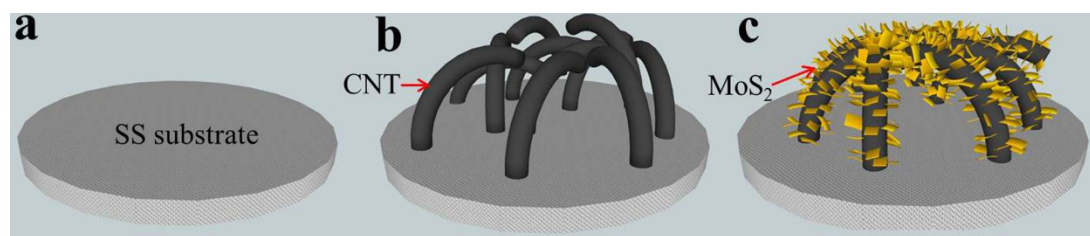


Fig. S1 Fabrication processes of CNT/MoS₂ composite: (a) Stainless steel (SS) substrate preparation; (b) Growth of CNTs onto the SS substrate; (c) Synthesis of MoS₂ flakes onto the CNT surface.

1.1 Growth of CNTs

After sequentially ultrasonic cleaned in acetone, isopropyl alcohol and de-ionized (DI) water, SS chips with the

diameter of 1.5 cm were blew by N₂ and baked in oven. 8 nm Nickel (Ni) films were deposited onto the chips as catalyst by electron beam evaporation (Auto 306, HHV system). The chips were then put in a home-made furnace for CNT growth in the atmosphere of 180 sccm Ar and 70 sccm H₂. Once temperature was ramped up to 700 °C, ethanol vapor was introduced into furnace as carbon sources for CNT formation. After 15 minutes' growth, ethanol vapor was cut off and the furnace was cooled down to room temperature. The SS chips were covered by black layer of CNTs.

1.2 Synthesis of MoS₂

The SS supported CNT samples were firstly treated by O₂ plasma at RF power of 30 W for 10 seconds before the synthesis of MoS₂. The back sides of SS were protected by Polytetrafluoroethylene (PTFE) tapes. Samples were then put in 20 ml Teflon-lined SS autoclaves with 6 mL ammonium tetrathiomolybdate (purity 99.95%, Sigma Aldrich) solution and kept at 200 °C for 10 hours. After cooled down to room temperature naturally, the samples were rinsed several times by de-ionized (DI) water followed by baking at 60 °C for 8 hours. Finally, the samples were annealed at 500 °C for 2 hours with Ar and H₂ as the protection atmosphere.

1.3 Electrochemical characterization

The obtained composite on SS substrates was directly assembled into CR 2032 type half cells while pure Li foils were used as the counter electrodes. The half cells were assembled in a glove box filled with pure Ar (Innovative Technology, Inc.). The electrolyte was LiPF₆ (1.0 M) dissolved in ethylene carbonate and diethyl carbonate (EC/DEC, 1:1 by volume). The half cells were tested with galvanostatic charge and discharge cycling over the potential range of 0.01-3.0 V vs. Li/Li⁺ in a battery tester (NEWARE BTS-5 V, Neware Technology Co., Ltd.). Cyclic voltammetry (CV) test and electrochemical impedance spectroscopy (EIS) were carried out using Solartron

1287/1255B Electrochemical Interface. The CNT mass loadings were determined by weighing the samples before and immediately after the CVD growth using an analytical balance (Mettler Toledo XP 26, 0.002 mg) while for MoS₂, weight was measured after the annealing process. The total mass of CNT/MoS₂ composite was around 1 to 1.3 mg on each sample, with CNT and MoS₂ mass ratio around 1:3 to 1:2. Current applied and capacities obtained were all calculated based on the mass of the composite.

1.4 Fabrication and testing of the control group

To verify the improvement by the binder-free constructing and CNTs contents, commercial MoS₂ powder (~6 µm particle size, Sigma Aldrich) was mixed with acetylene black and poly(vinylidene difluoride) (PVDF) binders at the weight ratio of 8:1:1 and tested under the same conditions for comparison. Besides, bare CNTs on SS substrates were also tested to evaluate CNTs' contribution in capacity.

1.5 Structural characterization

SEM images were taken by LEO 1550 Gemini field-emission scanning electron microscopy (FESEM). Transmission electron microscopy (TEM) was carried out in JEOL JEM-2100F (HR). Raman spectra were obtained using a WITec Raman system with a laser wavelength $\lambda=532$ nm.

2. Raman spectroscopy

The I_D/I_G ratio of as-synthesized CNTs is relatively high, probably because the relatively low growth temperature and high growth rates of the CNTs increase the possibility of disordering or vacancy of carbon atoms in the structure. Such defects are possible to serve as nuclei centers for MoS₂, which have already been proven in previous work of nanoparticles on CNTs.¹

3. TEM characterization of the CNTs grown by CVD.

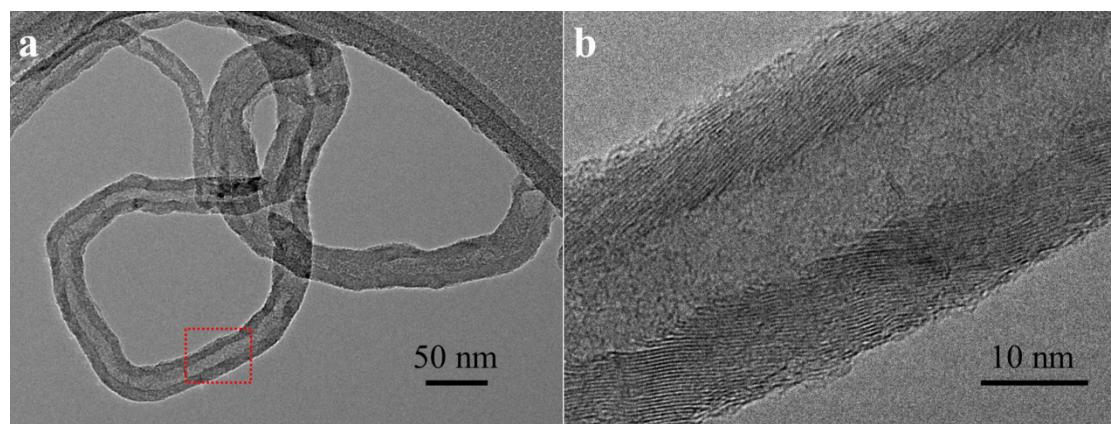


Fig. S2 TEM image of randomly selected CNTs after dispersion; (b) HRTEM image of the rectangle region in (a).

The CNTs clearly consist of tens of walls while cavities can be found in the axis, proving that the CNTs are multi-walled CNTs (MWCNTs).

3. XPS characterization of the CNT/MoS₂ composite

X-ray photoelectron spectroscopy (XPS) was carried out using a Thermo Scientific Theta Probe XPS. Monochromatic Al K α X-ray ($h\nu=1486.6\text{eV}$) was employed for analysis with an incident angle of 30° with respect to surface normal. Photoelectrons were collected at a take-off angle of 50° with respect to surface normal.

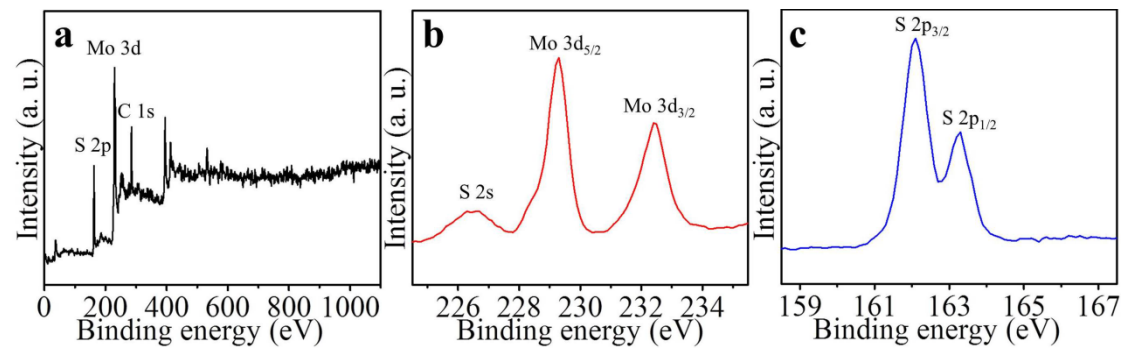


Fig. S3 XPS spectra of the CNT/MoS₂ composite: (a) survey scan and (b, c) high resolution scans of Mo 3d and S 2p, respectively.

As shown in Fig. S3 (b), the binding energy profile of Mo 3d shows two strong peaks at 229.3 and 232.4 eV which

can be attributed to Mo 3d_{5/2} and Mo 3d_{3/2} while in Fig. S3 (c), S 2p_{3/2} and S 2p_{1/2} peaks clearly exhibit at 162.1 and 163.3 eV, respectively.^{2, 3} Hence, the XPS data further ascertains the successful synthesis of the MoS₂ material.

3. Energy-dispersive X-ray spectroscopy (EDX) line scan

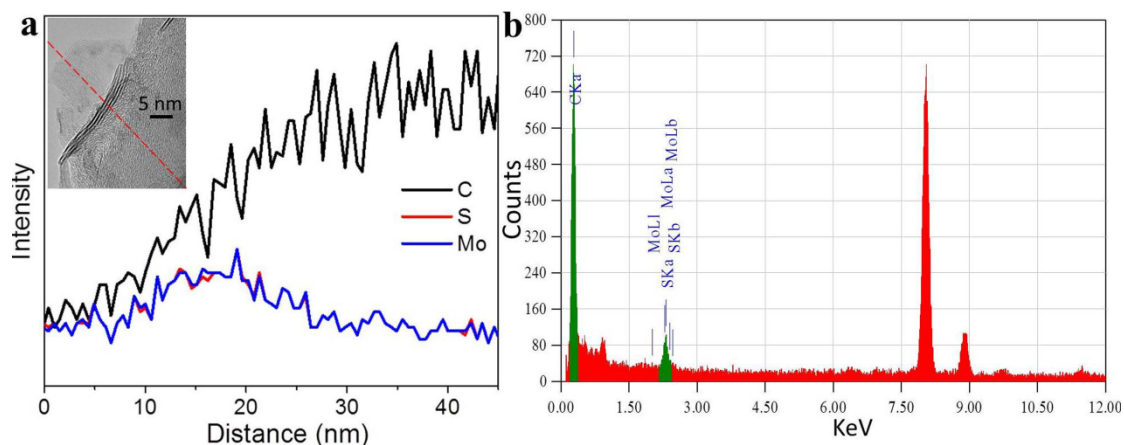


Fig. S4 EDX results. (a) Distribution of C, S and Mo elements across the MoS₂/CNT interface (inset indicates the scanning route); (b) Element composition of the scanned area. (Copper signal comes from the supporting TEM grid.)

The difference in element distribution from shell to core parts of the nanowires is clearly displayed. Carbon content increases towards the axis of the nanowire, which is the signal from CNT.

4. X-ray Diffraction (XRD)

XRD signal was collected by powder XRD (Max 18 XCE, Japan) with a Cu K α source ($\lambda=0.154056$ nm).

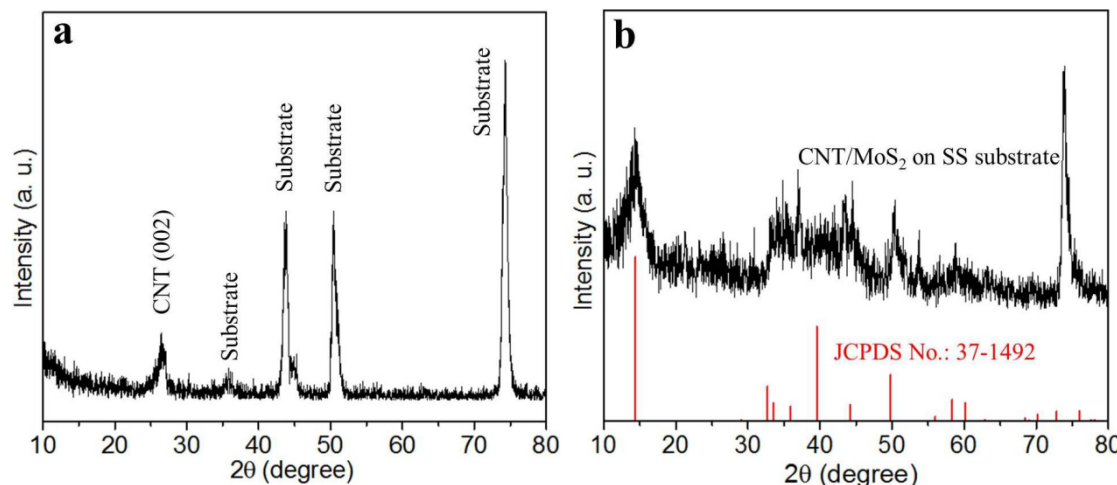


Fig. S5 XRD patterns of the CNT (a) and CNT/MoS₂ composite (b) on SS substrate, respectively.

The crystallographic structures of the CNTs and MoS₂ are confirmed XRD analysis, as shown in Fig. S5. Although the signal from SS substrate is very strong, yet the phases of CNTs and hexagonal MoS₂ (JCPDS No.: 37-1492) can still be observed.

5. Comparison between binder-free CNT/MoS₂ composite and commercial MoS₂ powder with binders.

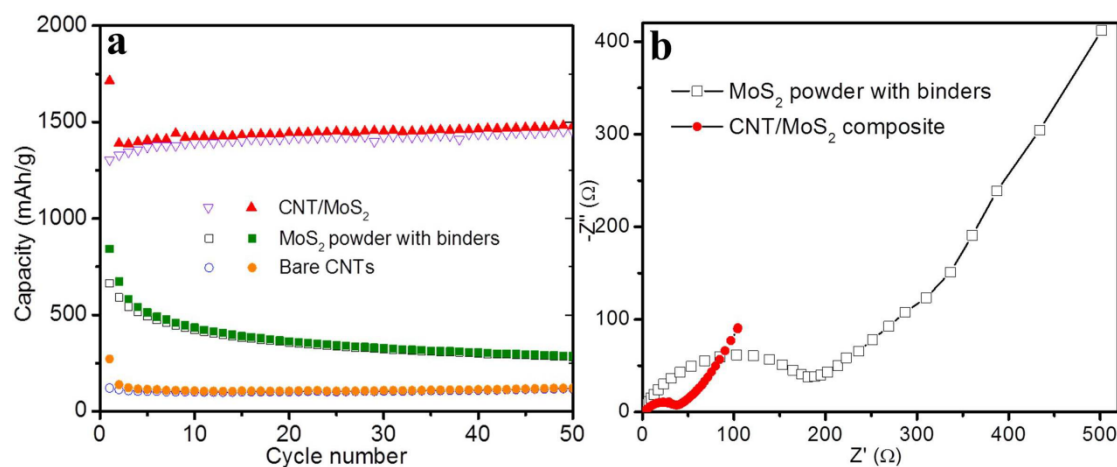


Fig. S6 (a) Specific de-lithiation (hollow) and lithiation (solid) capacities of binder-free CNT/MoS₂ composite (triangle), commercial MoS₂ particles with binders (square) and bare CNTs (circle) versus cycle number charge/discharged at 200 mA/g; (b) Nyquist plots (100 kHz–50 mHz) of CNT/MoS₂ composite and MoS₂ powder.

As shown in Fig. S6 (a), in sharp contrast to the high and stable capacity of binder-free CNT/MoS₂ composite, MoS₂ powder with binders exhibits much lower capacity and the capacity drops rapidly, indicating the superiority

of the binder-free architecting and also combination with CNTs. In addition, bare CNTs on the current collector only demonstrate a limited capacity below 200 mAh/g. Thus, the high capacity demonstrated by CNT/MoS₂ probably comes from the MoS₂ content and also the strong synergistic effects of MoS₂ and CNTs.⁴ As shown in Fig S6 (b), diameter of the semi-circle in Nyquist plot at high frequencies is significantly reduced in CNT/MoS₂ composite as compared to MoS₂ powder with binders. It proves that in the binder-free CNT/MoS₂ composite, internal resistance is remarkably reduced because of the direct and efficient electrical pathways between active material and current collector constructed by the highly conductive CNT networks. Transfer of electrons can be promoted dramatically during cycling, which contributes to the improved performance.⁵

6. Larger version of Fig. 3 in manuscript for a better identification

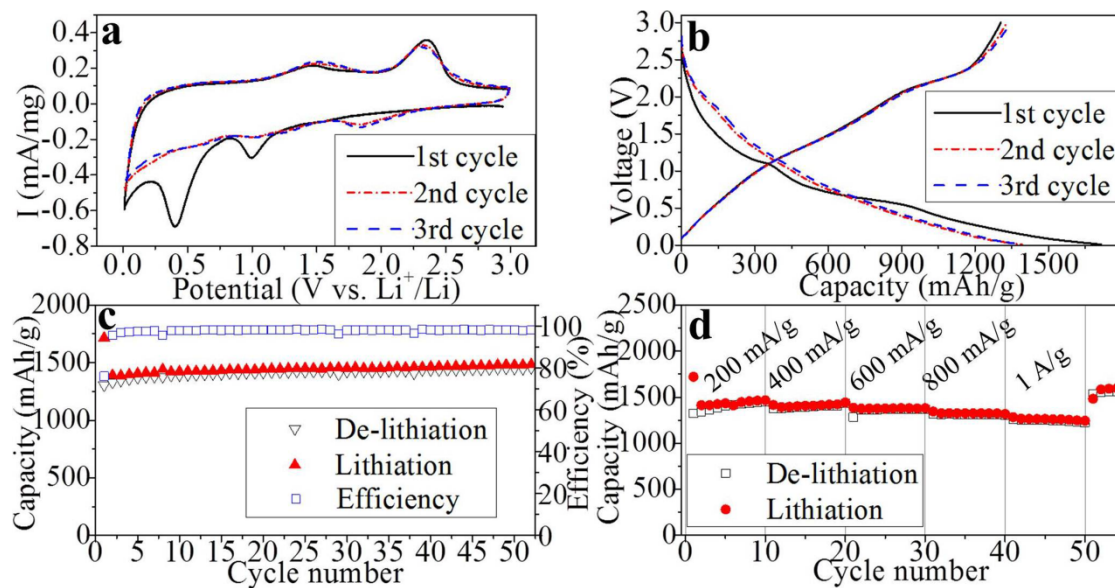


Fig. S7 (a) Cyclic voltammograms of the CNT/MoS₂ composite for the first 3 cycles measured at a scan rate of 0.1 mV/s between 0.01 V and 3 V; (b) Voltage capacity profiles of CNT/MoS₂ composite at current density of 200 mA/g; (c) Specific capacities and Columbic efficiency of the CNT/MoS₂ composite versus cycle number charge/discharged at 200 mA/g; (d) Charge/discharge capacities at different current rates.

References

1. P. Azadi, R. Farnood and E. Meier, *J. Phys. Chem. A*, 2009, **114**, 3962.
2. G. Eda, H. Yamaguchi, D. Voiry, T. Fujita, M. Chen and M. Chhowalla, *Nano Lett.*, 2011, **11**, 5111.
3. K.-K. Liu, W. Zhang, Y.-H. Lee, Y.-C. Lin, M.-T. Chang, C.-Y. Su, C.-S. Chang, H. Li, Y. Shi, H. Zhang, C.-S. Lai and L.-J. Li, *Nano Lett.*, 2012, **12**, 1538.
4. C. F. Zhang, Z. Y. Wang, Z. P. Guo and X. W. Lou, *ACS Appl. Mater. Interfaces*, 2012, **4**, 3765.
5. L. C. Yang, S. N. Wang, J. J. Mao, J. W. Deng, Q. S. Gao, Y. Tang and O. G. Schmidt, *Adv. Mater.*, 2013, **25**, 1180.